DYNAMIC SIMULATION OF BREAKAWAY AEROSTAT WITH EMERGENCY DEFLATION VALVES

Alap Kshirsagar[1#], Rajkumar S. Pant[2], Kowsik Bodi[3]

[1]*Junior Research Fellow(Project), Aerospace Engineering Department, IIT Bombay*
[2]*Professor, Aerospace Engineering Department, IIT Bombay*
[3]*Assistant Professor, Aerospace Engineering Department, IIT Bombay*
[#]*Corresponding author: Email - alapkshirsagar@gmail.com*

ABSTRACT: This paper presents a mathematical model for predicting the motion of an aerostat after tether breakage. Aerostats are equipped with emergency deflation valves for safe recovery of payload in case of accidental tether breakage. The trajectory of breakaway aerostat depends on the number and locations of these valves. The dynamic simulation of the aerostat is done by setting up and solving equations of motion in three dimensional spaces, considering the effect of added mass, aerodynamic forces and wind velocity. The model is implemented in MATLAB and simulation results are generated for input data of a sample aerostat. Comparison of aerostat trajectories for different valve configurations is presented along with some inferences.

Keywords: Breakaway aerostat, Payload recovery device, Dynamic simulation

1. INTRODUCTION

A tethered aerostat is an aerial platform for mounting equipment like radars, relay units, transducers at heights up to around 4.5 km (15000 ft.) for surveillance and telecommunication over a wide range on the ground, which is normally not achievable by transmission tower. Aerostats operate at high altitudes and there is a high probability of its interaction with sudden unexpected weather transformation leading to gust or storm that may result in tether breakage. The breakaway aerostat will rise in uncontrolled manner and cause a severe security threat to air traffic. Also when it expands beyond the structural limit of the envelope material, it will burst, leading to sudden loss of buoyancy and thereafter high descent rate. This in turn can result in severe third party damage and also loss of costly equipment used as payload. To prevent this, every aerostat needs to be equipped with a rapid deflation device to prevent accidents in case of tether breakage.

Various types of payload recovery devices have been developed which differ slightly in their working principles though initiate the same action. Once the signal is sent for deflation, holes are created in aerostat envelope using valves or current carrying loops, to allow the LTA gas to escape which brings the aerostat back to ground. The number and positions of such emergency deflation devices on aerostat envelop determine the time taken by aerostat to reach ground and the impact velocity of the payload. To avoid damage to the payloads, the impact velocity should not be very high. Also the location of recovery point should not be very far away from the deployment point of aerostat. Thus it is important to predict the trajectory of an aerostat after tether breakage.

2. MATHEMATICAL MODEL OF BREAK-AWAY AEROSTAT

2.1 Description of the model

The trajectory simulation of a breakaway aerostat requires the development of dynamic model based on flight dynamics of the aerostat. The aerostat is modelled as a rigid or semi-rigid 6-DOF body, with three translation and three rotational degrees of freedom about mass center. Forces and moments on an aerostat in two dimensions are shown in Figure 1.

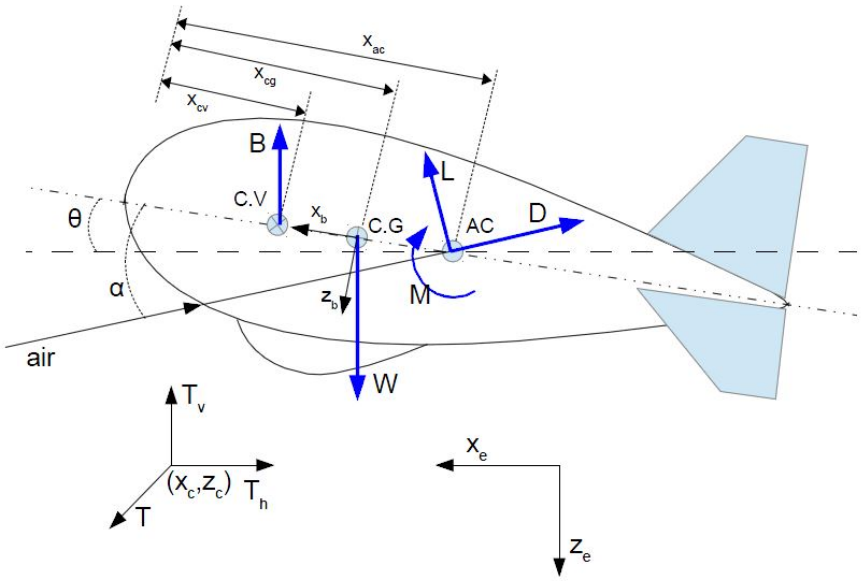

Figure 1: 2D Forces and Moments on an aerostat

The dynamic simulation of the aerostat is obtained by setting up and solving equations of motion in three dimensional spaces. The equation of motion is developed similar to the aircraft flight dynamics model. However, in the case of aerostats and airships, the mass of air displaced is significant with respect to the system mass and hence added mass effect needs to be considered similar to the formulations used in marine hydrodynamics.

2.2 Rigid body equation

is the position vector of the CG, is the position vector of the origin of the body axis system and is the vector from origin of body axis to CG (all defined in the inertial axis system), then position vector of CG in inertial axis system is given by:

(1)

Velocity in inertial frame can be given by the derivative of the position vector

(2)

Velocity in body axis system can then be defined as

(3)

Where, is the transformation matrix from inertial to body axis system. The derivative of a vector in a frame can be transformed to a different frame by following rule:

(4)

Assuming that derivative of position vector of CG in body axis system is zero, we get

(5)

Similarly, acceleration of the body in body axis can be obtained by taking the derivative of the velocity

(6)

This can then be used to write the force acting on the body according to Newton's Law

(7)

Similarly, moment equation can be derived as

(8)

Where, ***I*** is the inertia matrix about the body axis system and velocities are in body frame. Forces and moment can now be written in matrix form as:

(9)

Where, S(x) is skew symmetric matrix as: S(x) = for x =

Forces and moments can be better represented as

(10)

Where, and ***Eye(3)*** is a 3x3 identity matrix.

Total forces and moments consist of forces due to gravity, buoyancy, thrust, inertia, added mass and aerodynamics. Added mass and aerodynamic forces have been explained later.

(11)

The above set of equation for rigid body can be re-written in simplified form as:

(12)

Where, is the mass matrix and is the Coriolis force and centrifugal acceleration term and

(13)

2.3 Forces due to added mass

In fluid mechanics, added mass is the inertia added to the system because some volume of fluid surrounding the system moves along with it. For vehicles that displace large mass of fluid compared to its own mass like in aerostats, parachutes, submarines added mass effect becomes significant and hence cannot be neglected. Forces and moments due to added mass can be given by:

(14)

This can be re-written as

(15)

The first term of force due to added mass can be collected with the rigid mass matrix as:

(16)

The second term can also be transferred to get

(17)

This can be combined with Eq. (12) to get

(18)

For added mass calculation, we have assumed that the shape of aerostat approximately matches the prolate ellipsoidal shape. Added mass and inertia matrices for a prolate ellipsoidal shape can be found out using the expression given by Fossens [1]

(19)

Where, is the mass of the air displaced by the volume of the vehicle, the inertia factors and can be obtained as

(20)

Where, *a* and *b* are the axis length of the ellipsoid. and can be found out as follows

(21)

(22)

2.4 Aerodynamic forces on the aerostat

The current model uses a cross fin configuration for which the aerodynamic model presented was taken from work done by Mueller et. al [2]. Mueller used the procedure outlined by Jones and Delaurier [3] for aerodynamic coefficient estimation which has been verified for less than 30 degree angle of attack. As mentioned by Krishna et al. [4], as the aerostat breaks away from a statically stable tethered condition, the excess free lift pushes the aerostat upwards just after the breakage resulting in high angle of attack (~ -90) this calls for the modification to the model for high angle of attack, and hence appropriate corrections as suggested by Jorgensen [5] are made.

The forces are labelled as X, Y, Z and the moments about the nose as L, M, and N. Expressions here are derived for a cross fin configuration aerostat by Mueller [2] using the guidelines provided by Jones and Delaurier [3].

(23)

(24)

Z = (25)

L = (26)

M = (27)

N = (28)

The aerodynamic coefficients are defined below as:

(29)

(30)

(31)

(32)

(33)

(34)

(35)

(36)

(37)

These equations are valid for angle of attack less than 30 degrees so corrections are made to these as suggested by Jorgensen [5]. The values for simulation have been taken from studies on aerostat in the past by Delaurier [3] and Xiaohua [6].

2.5 Wind model

HWM-93 [7] is a comprehensive empirical model of wind fields based on the long-term historical observation data, retrieved data and other previous models, and they have an important complementary role and practical value in providing information of the middle atmosphere wind field, especially in regions with relatively lacking wind measurement stations. The variation of meridional (in the north south direction) and zonal (in the east-west direction) wind speed with altitude for Mumbai over various seasons as predicted by the *HWM-93* is show in Figure 2.

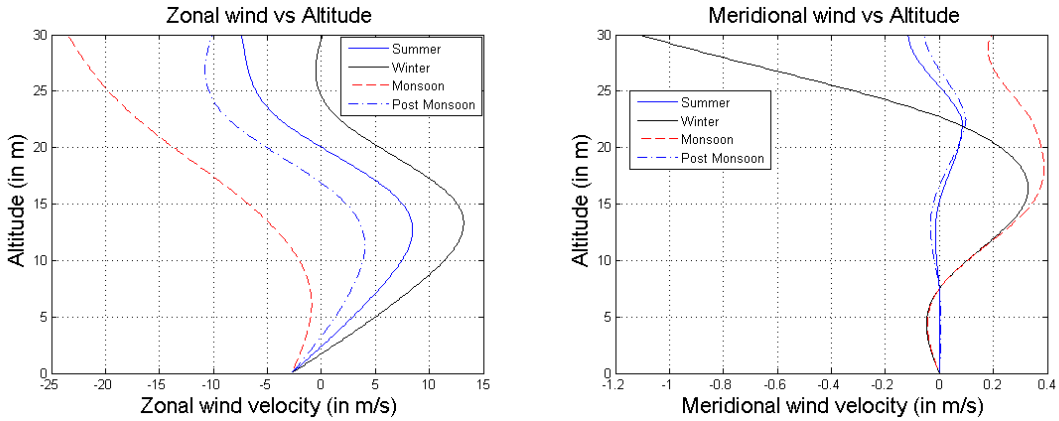

Figure 2: Seasonal variation of wind velocity with altitude

2.6 Assumptions in the model

The following assumptions have been made while carrying out the simulation results

1. The tether of aerostat breaks from a stable equilibrium position, i.e., the pitch angle of the aerostat is negligible
2. Aerostat is assumed to break-away from the topmost attachment point
3. Trajectory has been divided into two phases
    a. In the ascent phase, the aerostat hull is pressurized and maintains an aerodynamic shape, so a 6 DOF model is used
    b. During the descent phase most of the lifting gas has escaped and the shape of aerostat cannot be predicted, and hence a point mass model is assumed
4. During the descent phase, LTA gas does not leak from valves located at the bottom. Two reasons for this assumption are:
    a. As the aerostat descends the bottom surface experiences higher stagnant pressure and since the hull is flaccid the bottom surface will get curved towards inside (like a parachute) further creating high pressure zone. Hence, the internal gas does not leak under such circumstances

b. LTA gas has a tendency to move upward and will pressurize the top surface of the hull. This phenomenon is extensively used in zero-pressure balloon wherein an open valve is provided at the bottom of the spherical balloon and it slowly expands and inflates as it increases altitude without leaking from the bottom valve

5. A 10 second delay has been provided for detection of breakage and initiation of opening of valves and a valve gets fully opened within 5 seconds after initiation
6. As the gas leaks out mass and volume of the system changes. Moment of inertia is assumed to be directly proportional to $m_{total}V^{2/3}$
7. The effect of thrust due to gas coming out of the valves has been neglected. The validation of this assumption is presented in results section.

3. TRAJECTORY PLOTS FOR VARIOUS CONFIGURATIONS

The mathematical model is implemented in MATLAB. Dynamic simulation is carried out for a sample aerostat with input data as listed in Table 1. The GNVR shape [8-9] is assumed for the envelope of the aerostat.

Table 1: Input data for aerostat

Parameter	Values
Total Envelope Volume	3500 m^3
Operating Altitude (AMSL)	1000 m
Length	40 m
Max Diameter	13 m
Area of single fin (Including portion inside envelope)	130 m^2
Area of part of envelope included in (single) fin	12 m^2
Fin Height from envelope centreline	9 m
Fin root chord	8 m
Fin tip chord	3.3 m
Location of fin AC from envelope nose	35.5 m
Total envelope surface area (Hull only)	1290 m^2
Total wetted area of envelope	1644 m^2
Lateral projected area of envelope	396 m^2
Maximum all up weight of aerostat	1750 kg
Maximum payload capacity of aerostat	300 kg
Location of fin CP from envelope nose (assumed)	38 m
Specific Weight of tether	0.4 kg/m
Length of Tether	1500 m
Height of Center of Gravity from central axis	0 m
Location of Center of Gravity from envelope nose	24.84 m
Location of Center of Volume from envelope nose	19.78 m

Figure 3 shows the results of simulation for different number of holes on the bottom surface of aerostat's envelope. As shown in the figure, minimum 5 holes are required to keep the maximum altitude less than 6000 m.

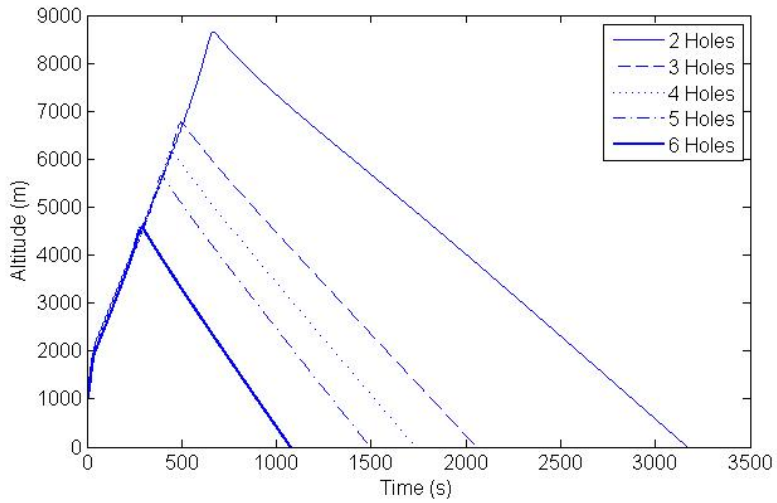

Figure 3: Variation of Altitude with Time for different number of holes

Based on this observation, we have selected following cases for simulations:

- Case 1: 5, 8 and 10 holes at the bottom (Hole Configurations 1, 3 and 5)
- Case 2: Case 1 with extra hole provided at the top (Hole Configurations 2 and 4)
- Case 3: Case 1 with multiple holes at the top (Hole Configurations 7 and 8)

The hole configurations are listed in Table 2.

Table 2: Hole Configurations

Hole Configuration	Description
1	5 Holes at the bottom
2	5 Holes at the bottom and 1 Hole at the top
3	8 Holes at the bottom
4	8 Holes at the bottom and 1 Hole at the top
5	10 Holes at the bottom
6	10 Holes at the bottom and 1 Hole at the top
7	5 Holes at the bottom and 2 Holes at the top
8	5 Holes at the bottom and 3 Holes at the top

3.1 Case-I: All holes at the bottom

In this case, all the valves are located at the bottom of the surface of the envelope. Three configurations have been considered as shown in Fig. 4-6. Configuration 1 has 5 holes, Configuration 3 has 8 holes and Configuration 5 has 10 holes.

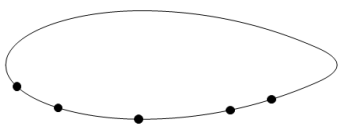

Figure 4: Configuration 1

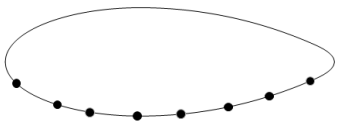

Figure 5: Configuration 3

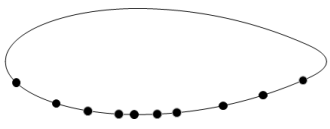

Figure 6: Configuration 5

Figures 7a to 7e present the simulation results for Case-1.

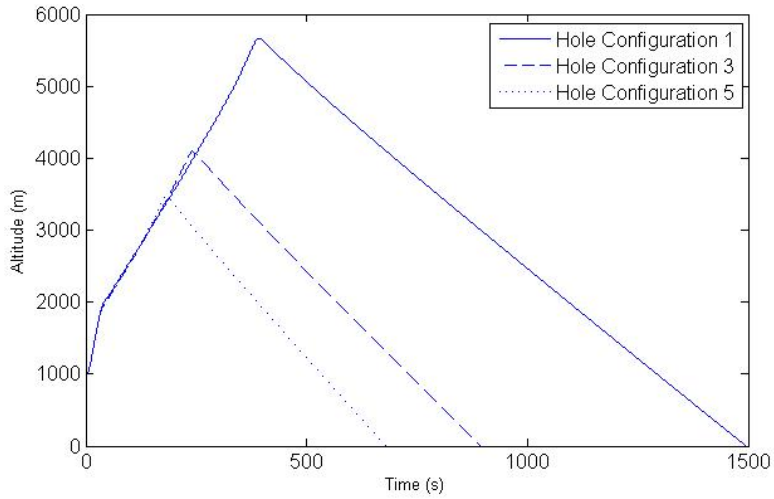

Figure 7a: Variation of Altitude with Time

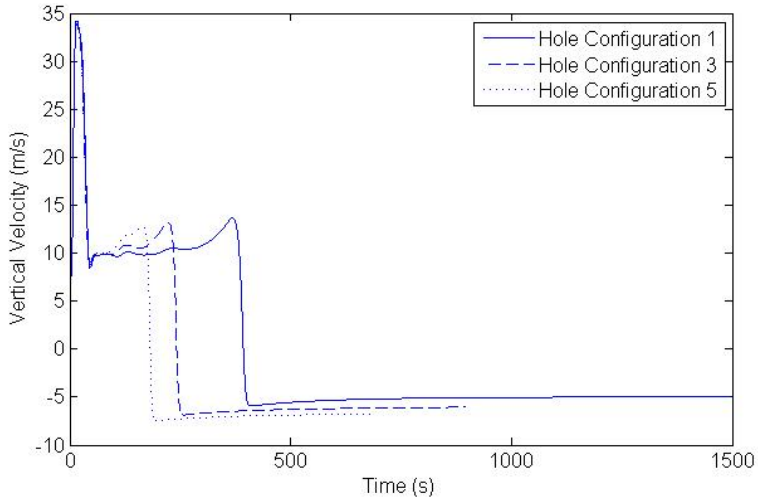

Figure 7b: Variation of Vertical Velocity with Time

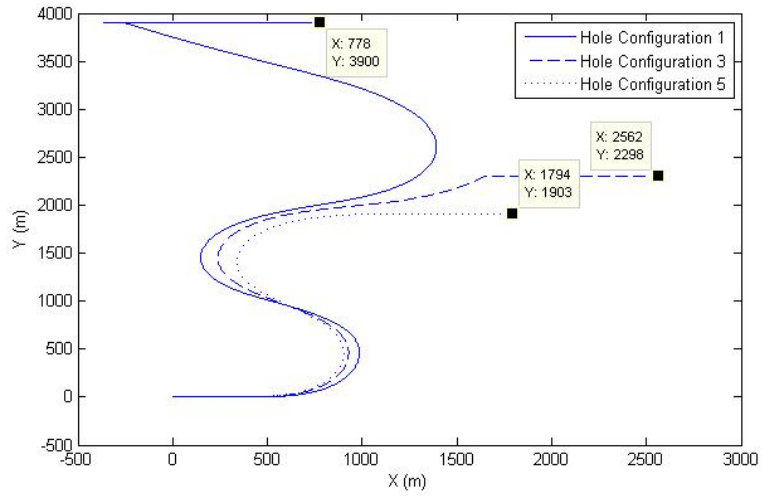

Figure 7c: Y vs. X Trajectory Co-ordinates

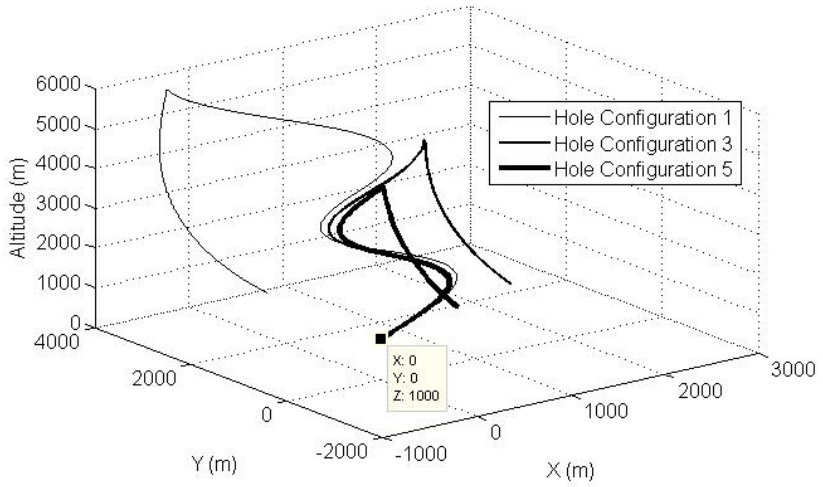

Figure 7d: 3D Trajectory

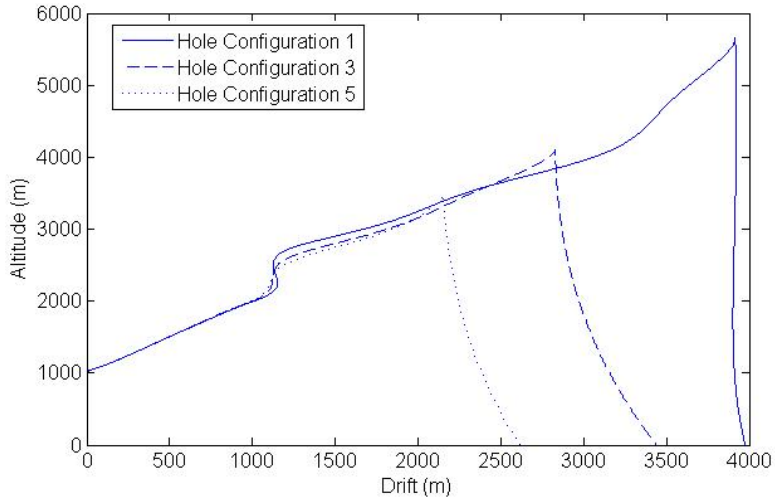

Figure 7e: Variation of Altitude with Drift

As seen from Figure 7b, the aerostat reaches the ground with an impact velocity less than 5 m/s for Configuration 3 and 5. The maximum altitude reached by the aerostat decreases with increase in number of holes, as shown in Figure 7a. The trajectory plots (Figure 7c and 7d) show that during ascent phase the aerostat follows a spiral path but during descent phase its motion is restricted to a plane, due to point mass model.

3.2 Case-II: Case I with extra valve provided at the top

In this case we consider configurations of Case-I with an extra hole provided at the top surface, as shown in Figures 8-10.

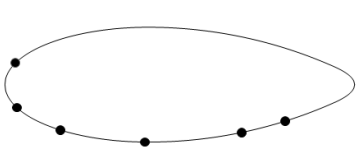

Figure 8: Configuration 2

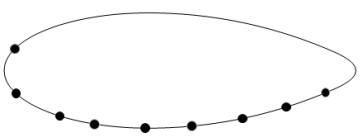

Figure 9: Configuration 4

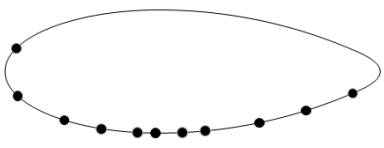

Figure 10: Configuration 6

Figures 11a to 11e present the simulation results for Case-II.

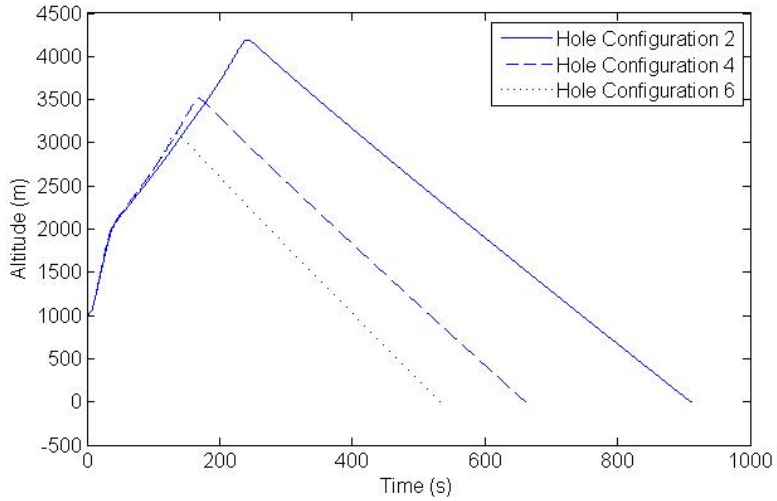

Figure 11a: Variation of Altitude with time

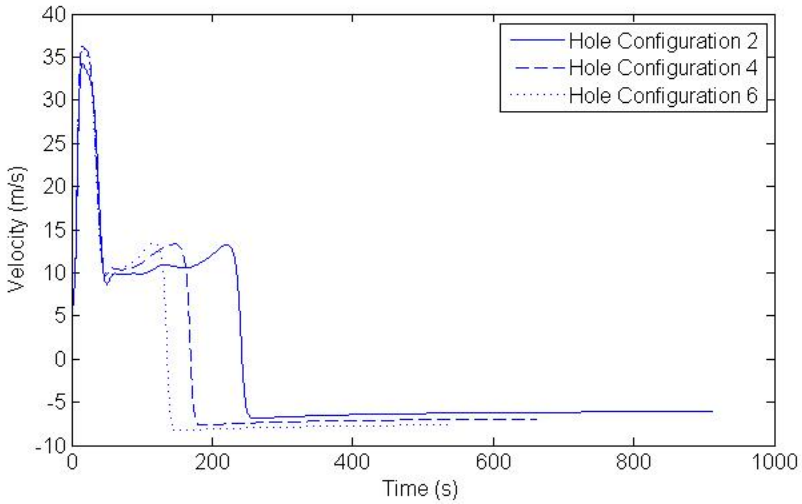

Figure 11b: Variation of Velocity with time

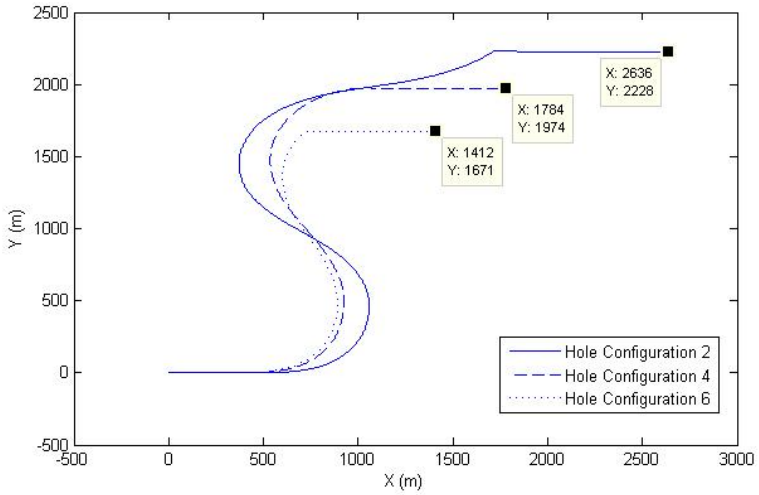

Figure 11c: Y vs. X Trajectory Co-ordinates

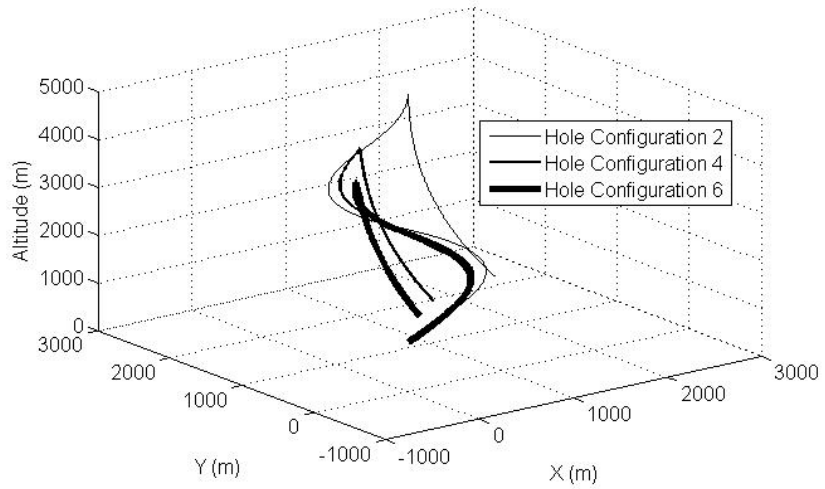

Figure 11d: 3D Trajectory

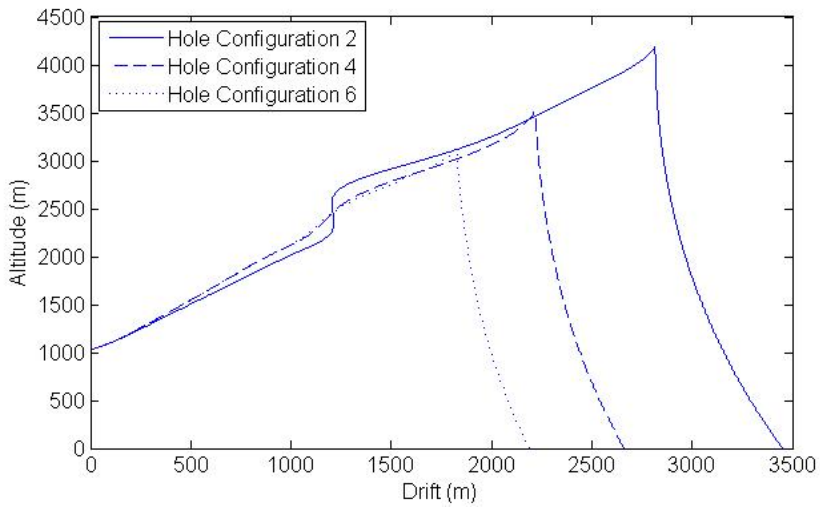

Figure 11e: Variation of Altitude with Drift

The results shown in Figures 11a to 11e are as expected, where the time to descend, maximum altitude and drift are significantly reduced as compared to Case-1. This is due to the additional hole provided at the top, through which the LTA gas keeps coming out during ascent as well as descent.

3.3 Case-III: Multiple valves at the top

In this case the number of holes at the top is increased further as shown in Figures 12 and 13. Both configurations have 5 holes at the bottom and configuration-7 has 2 holes at the top while configuration 8 has 3 holes at the top of aerostat.

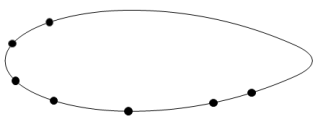

Figure 12: Hole Configuration 7

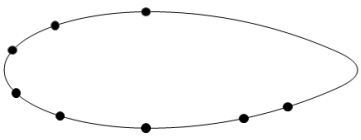

Figure 13: Hole Configuration 8

Figures 14a to 14e present the simulation results for Case-III.

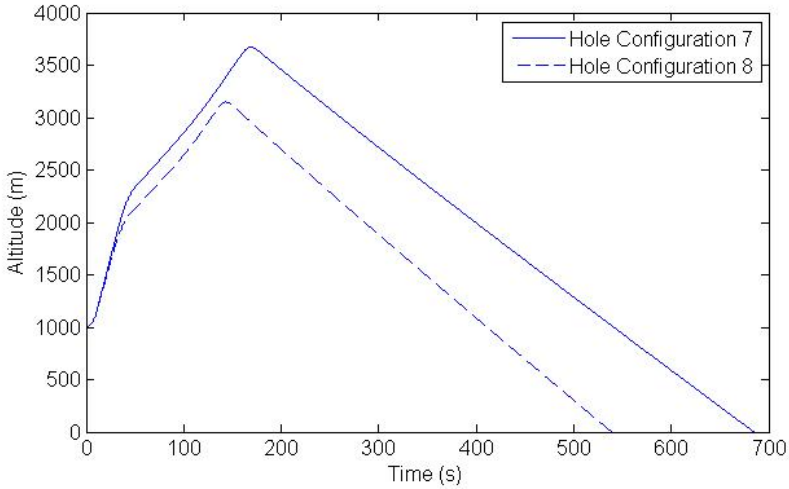

Figure 14a: Variation of Altitude with Time

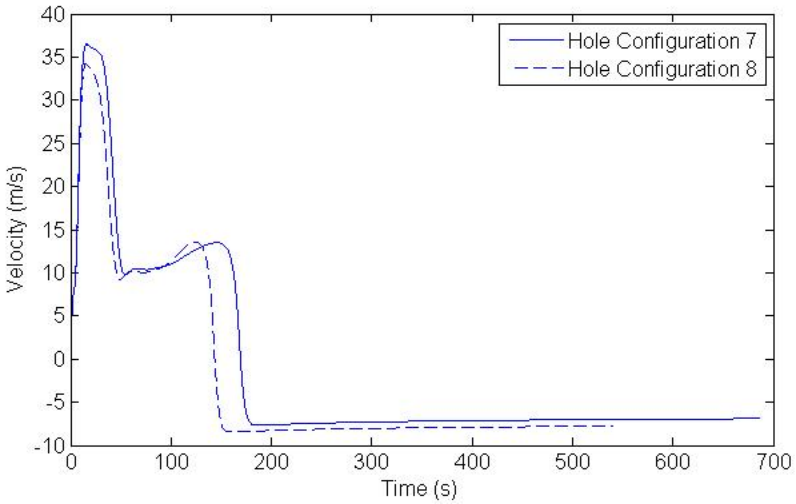

Figure 14b: Variation of Velocity with Time

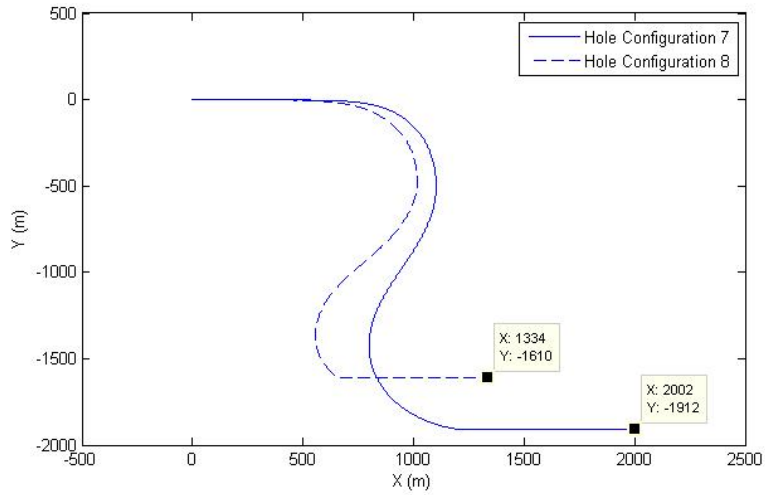

Figure 14c: Y vs. X Trajectory Co-ordinates

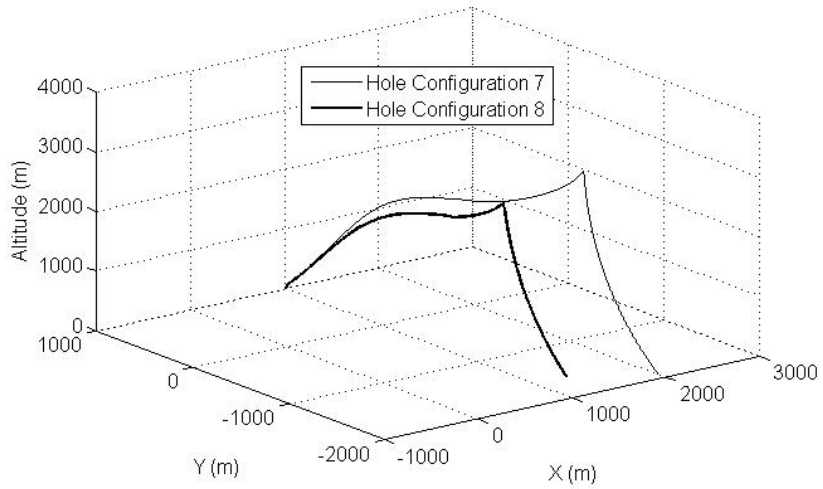

Figure 14d: 3D Trajectory

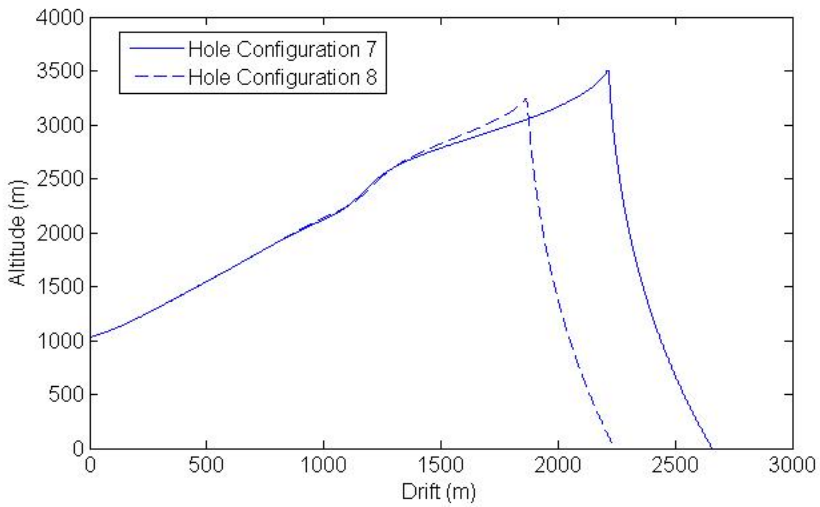

Figure 14e: Variation of Altitude with Drift

As can be seen from Figures 14 a and e, the time to descend, maximum altitude and drift decrease further as the number of holes on top is increased.

4. SUMMARY OF SIMULATION RESULTS

Table 3 presents a comparison of key parameters for different hole-configurations.

Table 3: Comparison of key parameters

Hole configuration	Maximum altitude (m)	Time to descend (s)	Drift (m)	Terminal velocity (m/s)
1	5664	1497	3977	4.9
2	4194	911	3451	6.1
3	4094	896	3442	6.1
4	3512	662	2661	6.9
5	3471	681	2616	6.7
6	3115	534	2188	7.6

7	3672	685	2768	6.9
8	3148	540	2091	7.7

The key observations that can be seen from the data reported in Table 3 are as follows:

- A minimum of 5 holes are required to keep the maximum altitude less than 6000 m.
- Maximum altitude reached by the aerostat decreases with increase in number of holes.
- Providing holes at the top decreases the maximum altitude, time to descend and drift.
- Hole configuration-8 has lowest drift, whereas hole configuration-6 has lowest maximum altitude.
- Hole configuration-1 has lowest terminal velocity, whereas hole configuration-6 has the lowest time to descend

CONCLUSION

The mathematical model of motion of aerostat after tether breakage, considering the effects of added mass, aerodynamic forces and wind model, is presented. Added mass effect is included by approximating the envelope to be of prolate ellipsoidal shape. Aerodynamic forces are estimated for cross-fin configuration. A comprehensive empirical model of wind fields, available in literature, is also included in the formulation. Sample simulation results are presented for an aerostat, with different configurations of emergency deflation valves. Results indicate that for limiting the maximum altitude reached by aerostat and impact velocity of payload on reaching ground, a minimum number of valves are required to be provided on aerostat. Also it is found that providing valves on top surface of the envelope is beneficial than providing valves on bottom surface. This dynamic simulation model can be used during conceptual design phase of an aerostat for determining the emergency deflation valve configuration. Also it can be used to predict the recovery point of payloads in case of accidental tether breakage of aerostats equipped with such payload recovery devices.

REFERENCES

1) Fossen, T. I., “Guidance and Control of Ocean Vehicles”, John Wiley and Sons, ISBN-13: 978-0471941132, 1994
2) Mueller, J. B., Paluszek, M. A. and Zhao, Y., “Development of an Aerodynamic Model and Control Law Design for a High Altitude Airship”, Collection of Technical Papers - AIAA 3rd "Unmanned-Unlimited" Technical Conference, Workshop, and Exhibit, Volume 1, 2004, Article no. AIAA 2004-6479, pp. 415-431, 2004
3) Jones, S. P. and DeLaurier, J. D., “Aerodynamics estimation techniques for aerostats and airships”, Journal of aircraft, vol. 20, no. 2, 1983
4) Krishna, R., Pant, R.S., and Bodi, K., “Dynamic Simulation of Breakaway tethered Aerostat including Thermal effects”, paper AIAA-2013-1341, Proceedings of 20th AIAA LTA Systems Technology Conference, Daytona Beach, FL, USA, March 25-27, 2013
5) Jorgensen, L. H., “Prediction of static aerodynamic characteristics for Space-Shuttle like and other bodies at angles of attack from 0^{o} to 180^{o}”, NASA TN D-6996, 1973

6) Xiaohua Z., “Static and dynamic simulation of a multi-tethered aerostat system" , Master’s dissertation, Department of Mechanical Engineering, Nanjing University of Aeronautics & Astronautics, China, 1994.

7) Sachs, P., “Wind Forces in Engineering”, Pergamon Press, ISBN-13: 978-0-08-021299-9, 1978

8) Narayana C. L. and Srilatha, K. R., “Analysis of aerostat configurations by panel methods”, BLISS project Document CF 0010, NAL, Bangalore, India, 2000

9) Sundaram, S., “Wind Tunnel Tests on 1:7 and 1:28 scale Aerostat models”, Technical Report, Experimental Aerodynamics Division, NAL, Bangalore, India, 2000.